

Article

Effect on Rotation Speed on Thermal Dehydration Characteristics of Waste Gypsum Particles in a Constant Volume Rotary Vessel by Heating

Koichiro Ogata ^{1,*}, Kotetsu Arimura ¹, Hayate Gotoh ¹, Kai Satoh ¹, Kazuki Tokumaru ¹ , Hideo Kawahara ²  and Hiroaki Sano ³

¹ Department of Mechanical Engineering, National Institute of Technology, Oita College, 1666 Maki, Oita 870-0152, Japan; k-tokumaru@oita-ct.ac.jp (K.T.)

² Department of Mechanical Systems Engineering, National Defense Academy, 1-10-20 Hashirimizu, Yokosuka 239-8686, Japan; kawahara@nda.ac.jp

³ Department of Civil and Environmental Engineering, National Defense Academy, 1-10-20 Hashirimizu, Yokosuka 239-8686, Japan; sano@nda.ac.jp

* Correspondence: k-ogata@oita-ct.ac.jp; Tel.: +81-975-552-6927

Abstract: This study examined the thermal dehydration characteristics of $\text{CaSO}_4 \cdot 2\text{H}_2\text{O}$ in a constant-volume rotary vessel. The experiment used $\text{CaSO}_4 \cdot 2\text{H}_2\text{O}$ particles obtained from the crushed waste gypsum board. The particle size ranged from 850 to 2000 μm , and the experiment was carried out at varying rotation speeds of 1, 10, and 35 rpm, with the vessel temperature heated to 180 °C. Temperature and pressure inside the vessel were measured simultaneously using the thermocouple and the pressure sensor. The XRPD measurement analyzed the transition of $\text{CaSO}_4 \cdot 2\text{H}_2\text{O}$ after the heating of particles. The result showed that the temperature growth rate was similar for high rotation speeds of 10 and 35 rpm, while periodic temperature changes occurred at the low rotation speed of 1 rpm. A distinguishing flow pattern was observed at the low rotation speed, and the particles inside the vessel collapsed periodically downward. This particle behavior was related to the temperature distribution of the rotation speed of 1 rpm. Additionally, the pressure in the vessel increased rapidly at higher rotation speeds. This trend indicates the desorption of the crystal water of $\text{CaSO}_4 \cdot 2\text{H}_2\text{O}$ due to the increasing temperature in the case of high rotation speed. Also, the XRPD measurement results showed the appearance of $\text{CaSO}_4 \cdot 0.5\text{H}_2\text{O}$ under the higher rotation speed conditions, and the mass fraction of $\text{CaSO}_4 \cdot 0.5\text{H}_2\text{O}$ increased with the rotation speed. Overall, the present study suggests that rotation speed plays a crucial role in determining the heat conduction and heat transfer of particles in a constant-volume rotary vessel.

Keywords: waste gypsum; constant-volume rotary vessel; heating; rotation speed; thermal dehydration



Citation: Ogata, K.; Arimura, K.; Gotoh, H.; Satoh, K.; Tokumaru, K.; Kawahara, H.; Sano, H. Effect on Rotation Speed on Thermal Dehydration Characteristics of Waste Gypsum Particles in a Constant Volume Rotary Vessel by Heating. *Materials* **2024**, *17*, 1276. <https://doi.org/10.3390/ma17061276>

Academic Editor: Sheikh A. Akbar

Received: 30 November 2023

Revised: 6 March 2024

Accepted: 7 March 2024

Published: 10 March 2024



Copyright: © 2024 by the authors. Licensee MDPI, Basel, Switzerland. This article is an open access article distributed under the terms and conditions of the Creative Commons Attribution (CC BY) license (<https://creativecommons.org/licenses/by/4.0/>).

1. Introduction

The gypsum board is made of a gypsum core material and is covered on both sides with base paper to create a flat panel. This type of board is known for its excellent fire resistance, sound insulation, heat insulation, and workability, making it an ideal building material. Additionally, it is great to see that flue gas desulfurization gypsum and wastepaper are also used as raw materials for gypsum boards, making them excellent recycled materials. Due to these advantages, the gypsum board is extremely popular as an interior base material for building walls, floors, and ceilings, and its production volume is increasing in Japan.

On the other hand, the quantity of waste gypsum boards generated from ageing buildings is increasing significantly. Unfortunately, most of these waste gypsum boards are disposed of in landfills. As a result, it is now considered controlled industrial waste due to instances where hydrogen sulfide has been produced in final disposal sites that handle waste gypsum boards in various locations. Consequently, processing waste gypsum boards

has become more expensive [1]. Under these circumstances, ongoing efforts are being made to convert $\text{CaSO}_4 \cdot 2\text{H}_2\text{O}$ produced from waste gypsum boards into $\text{CaSO}_4 \cdot 0.5\text{H}_2\text{O}$, which solidifies after being mixed with water and is used as a ground improvement material [2–9].

Generally, gypsum is transferred from $\text{CaSO}_4 \cdot 2\text{H}_2\text{O}$ to $\text{CaSO}_4 \cdot 0.5\text{H}_2\text{O}$ or CaSO_4 [10]. Research is also underway on the conversion of gypsum on Mars [11]. It is well known that a heating device converts $\text{CaSO}_4 \cdot 2\text{H}_2\text{O}$ to $\text{CaSO}_4 \cdot 0.5\text{H}_2\text{O}$ or CaSO_4 . Different heating devices such as rotary kilns [2] and electric furnaces [3,4] are commonly used, while far-infrared-type [5] devices have also been developed. For example, the gypsum is rotated and dispersed inside the kiln and dried using radiant heat from the burner flame and hot air in the case of a rotary kiln [2]. In addition, $\text{CaSO}_4 \cdot 2\text{H}_2\text{O}$, discharged by separating and crushing waste gypsum boards into paper and gypsum, has a broad particle size distribution ranging from 2 mm or less to several tens of micrometers. Therefore, it is crucial to treat gypsum boards via temperature management and heating control during the manufacturing process of $\text{CaSO}_4 \cdot 0.5\text{H}_2\text{O}$ [4].

Since $\text{CaSO}_4 \cdot 0.5\text{H}_2\text{O}$ solidifies with water, it is ideal to convert all $\text{CaSO}_4 \cdot 2\text{H}_2\text{O}$ to $\text{CaSO}_4 \cdot 0.5\text{H}_2\text{O}$ from the perspective of reusing gypsum. However, it has been pointed out that non-uniform heating of $\text{CaSO}_4 \cdot 2\text{H}_2\text{O}$ in the heating device occurs due to a large amount of $\text{CaSO}_4 \cdot 2\text{H}_2\text{O}$ being heated simultaneously [5,7]. For this purpose, equipment using rotary kiln heating and a reacting tank have been developed [2]. Although this method has improved the production rate of $\text{CaSO}_4 \cdot 0.5\text{H}_2\text{O}$, some $\text{CaSO}_4 \cdot 2\text{H}_2\text{O}$ remains after heat treatment [2]. This is because $\text{CaSO}_4 \cdot 2\text{H}_2\text{O}$ that is handled has a broad particle size distribution. Additionally, the drying characteristics of gypsum due to the heating applied to $\text{CaSO}_4 \cdot 2\text{H}_2\text{O}$ are unclear. Furthermore, the conversion characteristics of $\text{CaSO}_4 \cdot 2\text{H}_2\text{O}$ to $\text{CaSO}_4 \cdot 0.5\text{H}_2\text{O}$ have yet to be elucidated when temperature and pressure change.

This study evaluated the conversion characteristics of $\text{CaSO}_4 \cdot 2\text{H}_2\text{O}$ produced from waste gypsum boards to $\text{CaSO}_4 \cdot 0.5\text{H}_2\text{O}$. The test equipment used was a closed constant-volume rotary heating device to vary the temperature, pressure, and rotational speed. This paper discusses the results of investigating the thermal dehydration properties of $\text{CaSO}_4 \cdot 2\text{H}_2\text{O}$ when the particle size and initial filling mass of gypsum are kept constant, and the heating temperature, pressure, and rotational speed inside the vessel are varied.

2. Experiment

2.1. Experimental Equipment

Figure 1 shows this study's schematic diagram of constant-volume rotary heating equipment. The rotating vessel in the figure has an elliptical shape, and the sealed state is achieved by closing the pressure valve and sample insertion port. In the experiment, $\text{CaSO}_4 \cdot 2\text{H}_2\text{O}$ was naturally filled into a vessel, which was sealed and heated while rotating. LP gas was used as the heating source. The rotational motion of the rotating vessel was provided using a motor, pulley, and belt. A thermocouple (Hakko Denki, Nagano, Japan) and a pressure sensor (Krone, KDM30, Tokyo, Japan) were used to measure the temperature and pressure inside the rotating vessel. The temperature and pressure data sampling frequency are 1 s and 1.98 s, respectively. The sampling frequency difference depends on the different types of data loggers used to measure the temperature and the pressure. In this measurement, the beginning of the recording time for these sensors was the same. Then, we could obtain the time history data of the temperature and the pressure inside the rotating vessel. In addition, qualitative and quantitative analyses were performed using an X-ray powder diffraction device (Rigaku, MiniFlex 600, Tokyo, Japan) to investigate the conversion state of gypsum after heating.

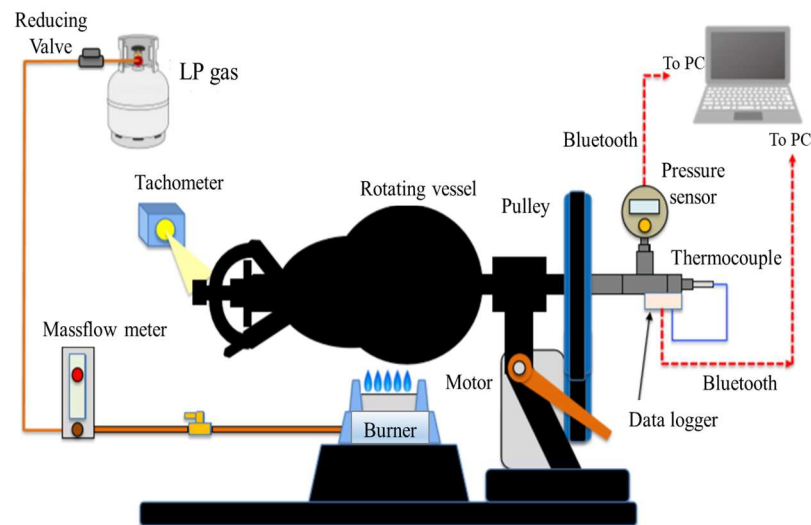


Figure 1. Material heating equipment using a constant-volume rotary vessel.

2.2. Particles Used and Experimental Conditions

The particles used in this study were $\text{CaSO}_4 \cdot 2\text{H}_2\text{O}$ derived from a waste gypsum board, with a particle size of less than $2000 \mu\text{m}$, collected from industrial waste treatment facilities in Okinawa Prefecture. In this study, the raw powder of $\text{CaSO}_4 \cdot 2\text{H}_2\text{O}$ was sieved to adjust the particle size to a range from 850 to $2000 \mu\text{m}$. The material density was 2376 kg/m^3 .

The volume of the elliptical rotating container shown in Figure 1 was 1450 cm^3 . In this study, the initial filling mass of powder was 100 g . The fuel flow rate was set to 1.2 L/min . Heating experiments were conducted with the rotation speed set at 1 , 10 , and 35 rpm .

3. Results

3.1. Conversion Characteristics of Gypsum

Figure 2 shows an example of the results of a heating experiment using constant-volume rotary heating equipment. The first vertical axis is the temperature inside the vessel, the second is the gauge pressure, and the horizontal axis is the heating time. The initial filling mass of particles was 100 g , the rotation speed was 35 rpm , and the heating end temperature was set to 100 , 130 , 150 , and $180 \text{ }^\circ\text{C}$. The figure shows that the slope of temperature and pressure against heating time is almost constant until around 300 s in region I. It is thought that an increase in internal energy due to heating occurred in this region. Next, in region II in the figure, the temperature gradient is almost constant as in region I, but there is a tendency for the pressure to increase from around 350 s . The temperature at this time was around $110 \text{ }^\circ\text{C}$, and the pressure was increased. It is inferred that steam was generated in the vessel due to the desorption of crystallized water from $\text{CaSO}_4 \cdot 2\text{H}_2\text{O}$ [12]. After that, in region III, from 450 s to around 530 s , the slopes of temperature and pressure concerning time are smaller than in region II. Since the internal temperature of the vessel in this region is between $130 \text{ }^\circ\text{C}$ and $150 \text{ }^\circ\text{C}$, it is assumed that evaporation of the crystallized water of $\text{CaSO}_4 \cdot 2\text{H}_2\text{O}$ was active, and the state changed to $\text{CaSO}_4 \cdot 0.5\text{H}_2\text{O}$. When further heating continued, the temperature and pressure inside the vessel rose rapidly, and it appeared that the vessel transitioned to a superheated steam state.

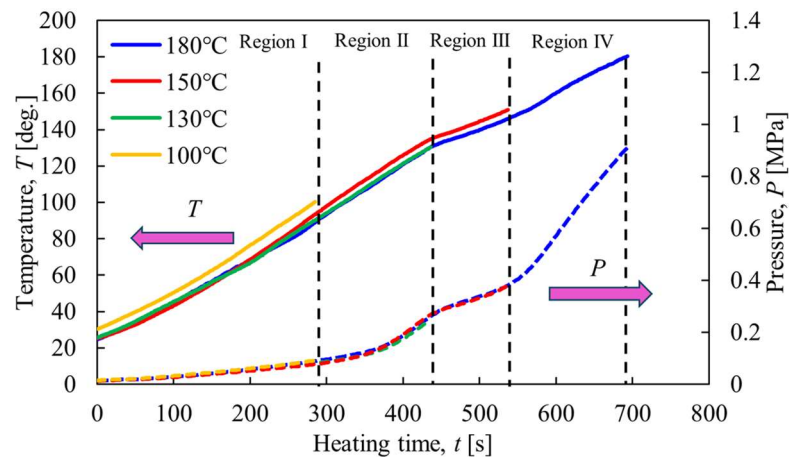


Figure 2. Time histories of temperature and pressure inside the rotary vessel.

Figure 3 shows the results of the XRPD measurements. The peak intensities at 12° and 21° in the figure represent $\text{CaSO}_4 \cdot 2\text{H}_2\text{O}$, and the 15° peak represents $\text{CaSO}_4 \cdot 0.5\text{H}_2\text{O}$. Here, a temperature of 100°C , 130°C , 150°C , and 180°C corresponds to the results of regions I, II, III, and IV. The measurement result before heating indicates the original particles. As shown in the figure, the result of region I at a temperature of 100°C maintains the state of $\text{CaSO}_4 \cdot 2\text{H}_2\text{O}$, similar to the original particles. When the temperature reaches 130°C of region II, the peak intensity of $\text{CaSO}_4 \cdot 0.5\text{H}_2\text{O}$ appears. When the temperature comes to region III of 150°C , the peak intensity of $\text{CaSO}_4 \cdot 0.5\text{H}_2\text{O}$ exceeds the intensity of $\text{CaSO}_4 \cdot 2\text{H}_2\text{O}$. Furthermore, it can be confirmed that only the peak of $\text{CaSO}_4 \cdot 0.5\text{H}_2\text{O}$ appears when the heating temperature is up to 180°C . As described above, using closed rotary heating equipment, this experiment could capture the conversion of $\text{CaSO}_4 \cdot 2\text{H}_2\text{O}$ to $\text{CaSO}_4 \cdot 0.5\text{H}_2\text{O}$.

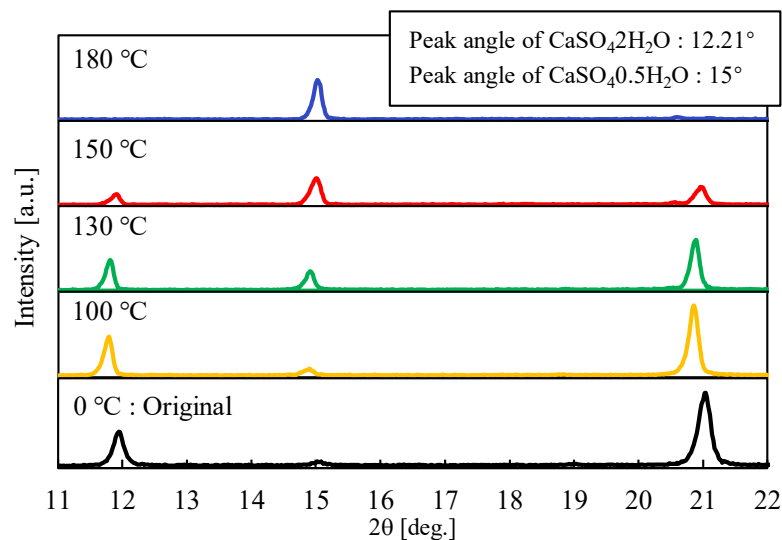


Figure 3. XRPD measurement results.

3.2. Effect of Rotation Speed on Conversion Characteristics of Gypsum

Figure 4 shows the relationship between the temperature and pressure inside the vessel against the heating time when the heating end temperature was 100°C . In addition, Figure 5 indicates the XRPD measurement results where the rotation speed of the vessel was varied to 1, 10, and 35 rpm. Figure 4 shows that the temperature and pressure increased with a constant slope when the rotational speed was 10 and 35 rpm. On the other hand, it was confirmed that the temperature changed periodically under a rotation speed of 1 rpm.

From the results in Figure 5, only the peak intensity of $\text{CaSO}_4 \cdot 2\text{H}_2\text{O}$ appeared when the heating temperature was 100°C , and no effect of change in rotation speed was observed.

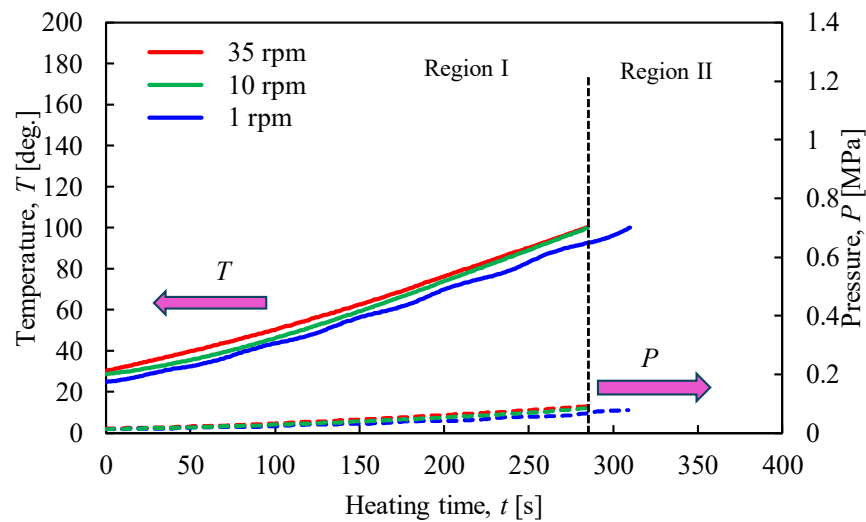


Figure 4. Time histories of temperature and pressure inside the rotary vessel at a heating end temperature of 100°C when the rotation speed was changed.

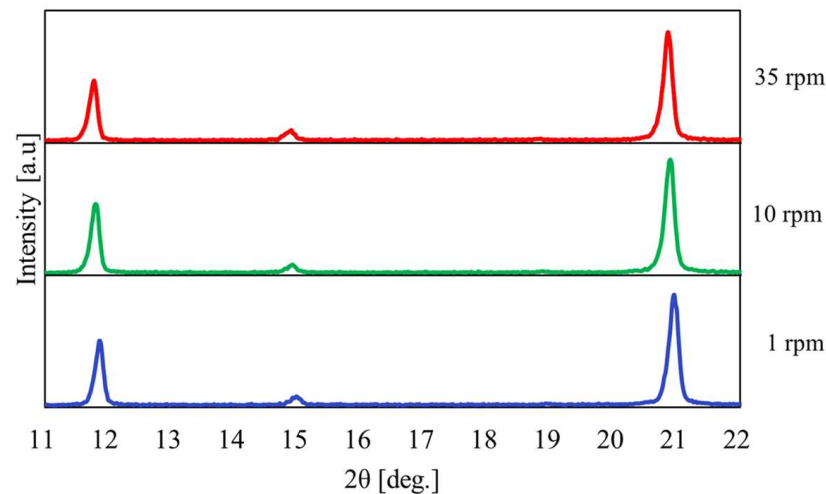


Figure 5. XRPD measurement results at a heating end temperature of 100°C when the rotation speed was changed.

Table 1 shows the mass fraction of $\text{CaSO}_4 \cdot 2\text{H}_2\text{O}$, $\text{CaSO}_4 \cdot 0.5\text{H}_2\text{O}$, and CaSO_4 at a heating end temperature of 100°C and a rotation speed of 1, 10, and 35 rpm. Here, the mass fraction of each kind of gypsum was determined by Rietveld analysis. The conditions where the rotation speed and temperature are zero indicate the measurement data of the gypsum before heating. In addition, Figure 6 shows a graph comparing measured mass fractions organized by each rotation speed. As shown in the figure, when the heating end temperature was 100°C , there was no significant difference in the mass fraction of gypsum even if the rotation speed changed. On the other hand, $\text{CaSO}_4 \cdot 2\text{H}_2\text{O}$ before heating contained $\text{CaSO}_4 \cdot 0.5\text{H}_2\text{O}$ and CaSO_4 . This is because the gypsum used in this study was a waste gypsum board, and it seems that these gypsums were generated during waste disposal.

Table 1. Results of the mass fraction of $\text{CaSO}_4 \cdot 2\text{H}_2\text{O}$, $\text{CaSO}_4 \cdot 0.5\text{H}_2\text{O}$, and CaSO_4 using Rietveld analysis at a heating end temperature of 100°C when the rotation speed was changed.

N (rpm)	T ($^\circ\text{C}$)	$\text{CaSO}_4 \cdot 2\text{H}_2\text{O}$ ϕ_m (%)	$\text{CaSO}_4 \cdot 0.5\text{H}_2\text{O}$ ϕ_m (%)	CaSO_4 ϕ_m (%)
0	0	93.74	4.14	2.13
1	100	87.30	6.18	6.52
10	100	89.49	6.96	3.56
35	100	85.44	8.44	6.22

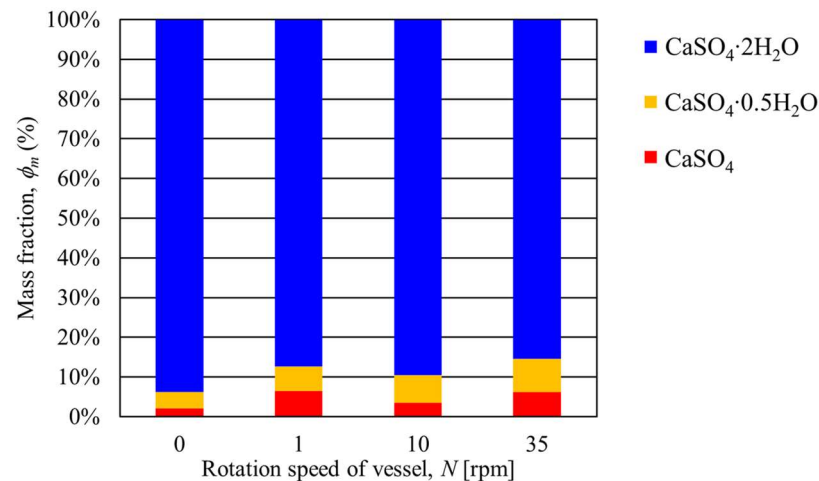
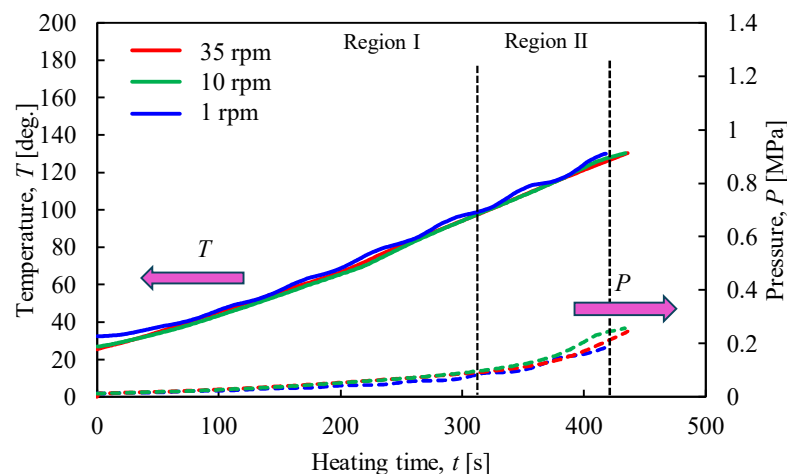
**Figure 6.** Relationship between the transferring mass fraction of gypsum and the rotation speed of the rotary vessel at a heating end temperature of 100°C .

Figure 7 shows the relationship between the temperature and pressure inside the vessel when the heating end temperature was 130°C . Figure 8 shows the results of the XRPD measurement. The rotation speed of the vessel was 1, 10, and 35 rpm. In Figure 7, the temperature gradient in region I appears almost constant when the rotation speed is 10 and 35 rpm. On the other hand, periodic changes in the temperature curve were confirmed under a rotation speed of 1 rpm. In region II, there was a tendency for the pressure to increase at all rotational speeds. From the XRPD measurement results in Figure 8, $\text{CaSO}_4 \cdot 0.5\text{H}_2\text{O}$ can be confirmed at all rotation speeds. This result indicates that the desorption of crystallized water from the $\text{CaSO}_4 \cdot 2\text{H}_2\text{O}$ has begun.

**Figure 7.** Time histories of temperature and pressure inside the rotary vessel at a heating end temperature of 130°C when the rotation speed was changed.

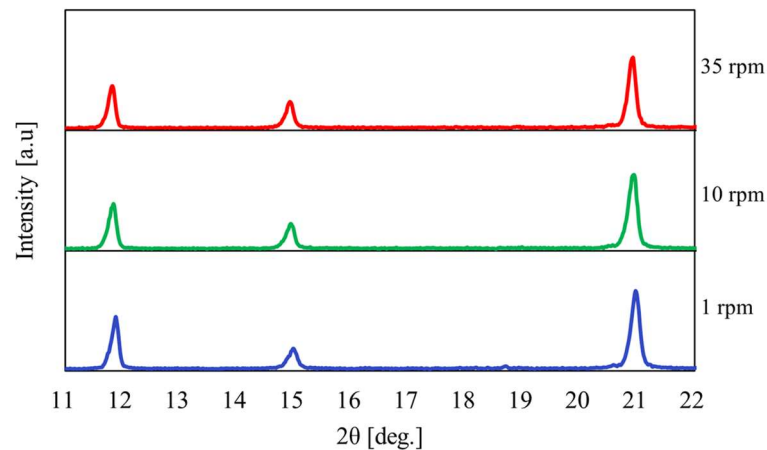


Figure 8. XRPD measurement results at a heating end temperature of 130 °C when the rotation speed was changed.

Table 2 shows the mass fractions of $\text{CaSO}_4 \cdot 2\text{H}_2\text{O}$, $\text{CaSO}_4 \cdot 0.5\text{H}_2\text{O}$, and CaSO_4 under the conditions that the heating end temperature was 130 °C and the rotation speed was 1, 10, and 35 rpm. In addition, Figure 9 shows the mass fraction of gypsum organized at each rotation speed. The figure shows that the mass fraction of $\text{CaSO}_4 \cdot 2\text{H}_2\text{O}$ at a rotation speed of 1 rpm decreased by 12.33% compared to without rotation. Additionally, the mass fraction of $\text{CaSO}_4 \cdot 0.5\text{H}_2\text{O}$ increased by 5.63% under the same condition. Next, no significant change in the mass fractions of $\text{CaSO}_4 \cdot 2\text{H}_2\text{O}$ can be confirmed between 1 rpm and 10 rpm rotation speeds. When the results of the rotation speeds of 1 rpm and 35 rpm were compared, the mass fraction of $\text{CaSO}_4 \cdot 2\text{H}_2\text{O}$ at a rotation speed of 35 rpm decreased by 9.52% compared to the result of the rotation speed of 1 rpm. Furthermore, the mass fraction of $\text{CaSO}_4 \cdot 0.5\text{H}_2\text{O}$ with a rotation speed of 35 rpm was 9.27% higher. These results show that although the amount is small, conversion from $\text{CaSO}_4 \cdot 2\text{H}_2\text{O}$ to $\text{CaSO}_4 \cdot 0.5\text{H}_2\text{O}$ begins when the heating end temperature is 130 °C.

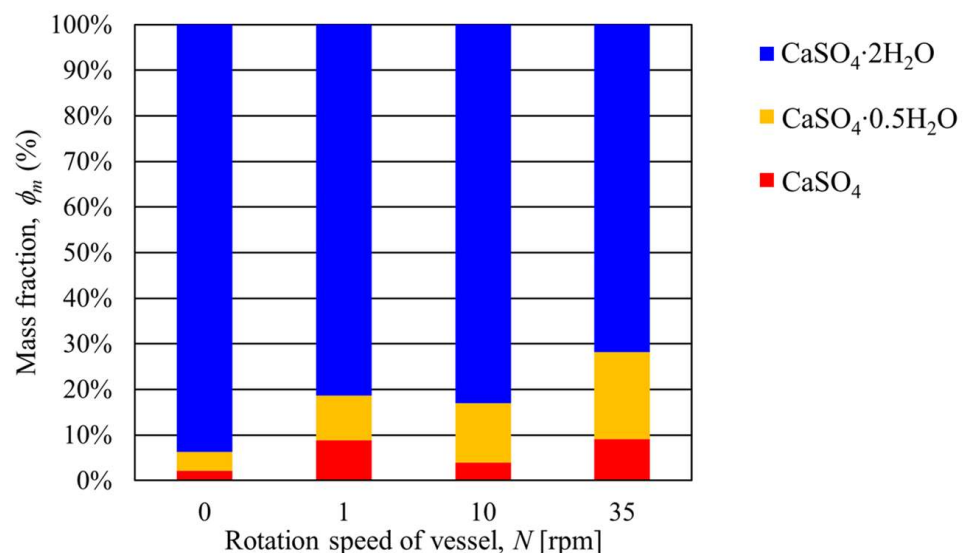


Figure 9. Relationship between the transferring mass fraction of gypsum and the rotation speed of the rotary vessel at a heating end temperature of 130 °C.

Table 2. Results of the mass fraction of $\text{CaSO}_4 \cdot 2\text{H}_2\text{O}$, $\text{CaSO}_4 \cdot 0.5\text{H}_2\text{O}$, and CaSO_4 using Rietveld analysis at a heating end temperature of 130°C when the rotation speed was changed.

N (rpm)	T ($^\circ\text{C}$)	$\text{CaSO}_4 \cdot 2\text{H}_2\text{O}$ ϕ_m (%)	$\text{CaSO}_4 \cdot 0.5\text{H}_2\text{O}$ ϕ_m (%)	CaSO_4 ϕ_m (%)
0	0	93.74	4.14	2.13
1	130	81.41	9.77	8.89
10	130	82.98	13.06	3.95
35	130	71.89	19.04	9.07

Figure 10 shows the relationship between the temperature and pressure inside the rotary vessel and the heating time when the heating end temperature was 150°C . Figure 11 shows the XRPD measurement results. The rotation speed of the vessel was varied between 1, 10, and 35 rpm. From Figure 10, periodic temperature changes were confirmed when the rotation speed was 1 rpm, similar to the heating end temperatures of 100°C and 130°C . The slope of temperature and pressure in region III tended to decrease more than in region II. Here, the pressure under a rotation speed of 35 rpm was higher than that under a low rotation speed. This suggests that the desorption of crystallized water from gypsum is promoted under conditions of high rotational speed. The XRPD results in Figure 11 also show that the peak intensity of $\text{CaSO}_4 \cdot 0.5\text{H}_2\text{O}$ increased as the rotation speed increased.

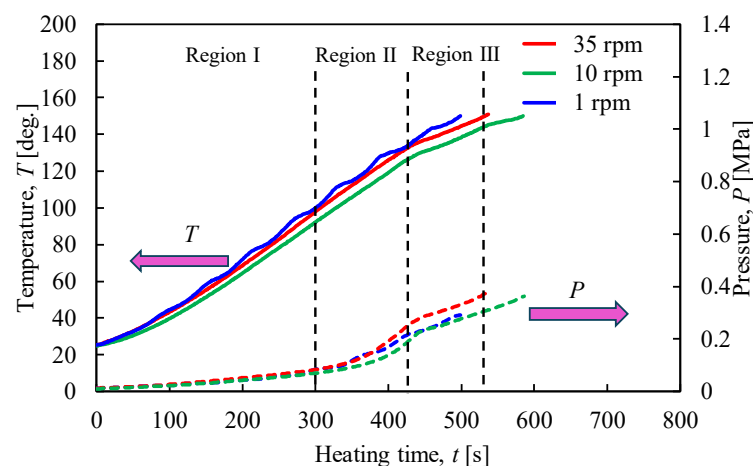


Figure 10. Time histories of temperature and pressure inside the rotary vessel at a heating end temperature of 150°C when the rotation speed was changed.

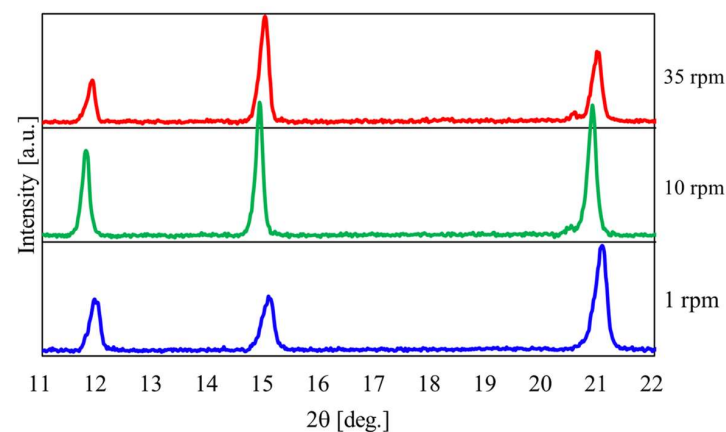


Figure 11. XRPD measurement results at a heating end temperature of 150°C when the rotation speed was changed.

Table 3 shows the mass fractions of $\text{CaSO}_4 \cdot 2\text{H}_2\text{O}$, $\text{CaSO}_4 \cdot 0.5\text{H}_2\text{O}$, and CaSO_4 when the heating end temperature was $150\text{ }^\circ\text{C}$ and the rotation speed was varied. Figure 12 shows the results of the mass fraction of gypsum at each rotation speed. The figure shows that when the heating end temperature was $150\text{ }^\circ\text{C}$ and the rotation speed was 1 rpm, the mass fraction of $\text{CaSO}_4 \cdot 0.5\text{H}_2\text{O}$ was 38.58%, indicating that $\text{CaSO}_4 \cdot 2\text{H}_2\text{O}$ was converted to $\text{CaSO}_4 \cdot 0.5\text{H}_2\text{O}$. Next, there was no significant difference in the mass fractions of $\text{CaSO}_4 \cdot 0.5\text{H}_2\text{O}$ when the rotation speeds were 10 rpm and 35 rpm. On the other hand, these mass fractions of $\text{CaSO}_4 \cdot 0.5\text{H}_2\text{O}$ increased by about 13% compared to the result of the rotation speed of 1 rpm. The above results show that the conversion from $\text{CaSO}_4 \cdot 2\text{H}_2\text{O}$ to $\text{CaSO}_4 \cdot 0.5\text{H}_2\text{O}$ is promoted by increasing the rotation speed.

Table 3. Results of the mass fraction of $\text{CaSO}_4 \cdot 2\text{H}_2\text{O}$, $\text{CaSO}_4 \cdot 0.5\text{H}_2\text{O}$, and CaSO_4 using Rietveld analysis at a heating end temperature of $150\text{ }^\circ\text{C}$ when the rotation speed was changed.

N (rpm)	T ($^\circ\text{C}$)	$\text{CaSO}_4 \cdot 2\text{H}_2\text{O}$ ϕ_m (%)	$\text{CaSO}_4 \cdot 0.5\text{H}_2\text{O}$ ϕ_m (%)	CaSO_4 ϕ_m (%)
0	0	93.74	4.14	2.13
1	150	52.87	38.58	8.66
10	150	39.41	51.91	8.56
35	150	37.39	51.01	11.60

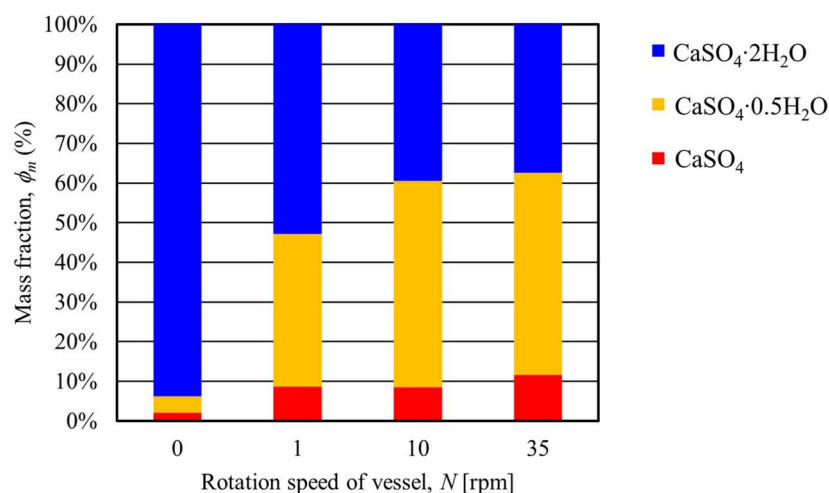


Figure 12. Relationship between the transferring mass fraction of gypsum and the rotation speed of the rotary vessel at a heating end temperature of $150\text{ }^\circ\text{C}$.

Figure 13 shows the relationship between the temperature and pressure inside the vessel concerning the heating time with the heating end temperature set at $180\text{ }^\circ\text{C}$. Figure 14 shows the results of the XRPD analysis at rotation speeds of 1, 10, and 35 rpm. In Figure 13, when the heating end temperature reaches $180\text{ }^\circ\text{C}$, the temperature and pressure gradients increase in region IV. In particular, the results show that the pressure increases rapidly as the rotation speed increases. As can be seen from the enlarged view of Figure 14b, under high rotational speed conditions, the peak intensity of $\text{CaSO}_4 \cdot 2\text{H}_2\text{O}$ no longer exists, and the conversion from $\text{CaSO}_4 \cdot 2\text{H}_2\text{O}$ to $\text{CaSO}_4 \cdot 0.5\text{H}_2\text{O}$ is promoted.

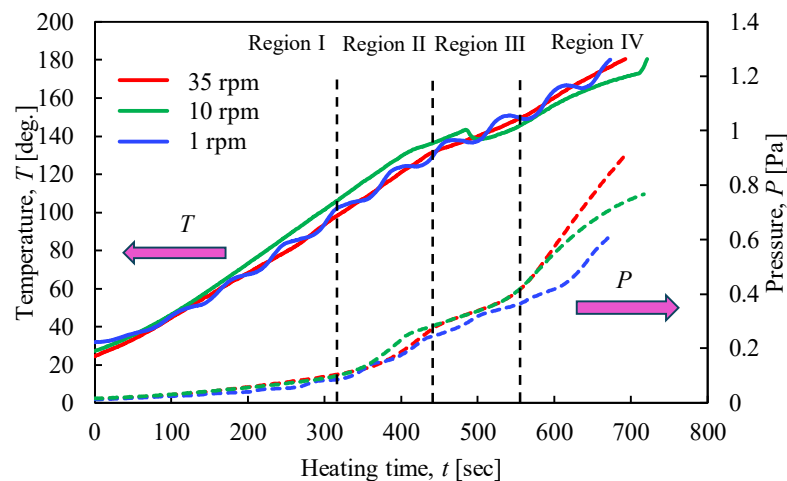
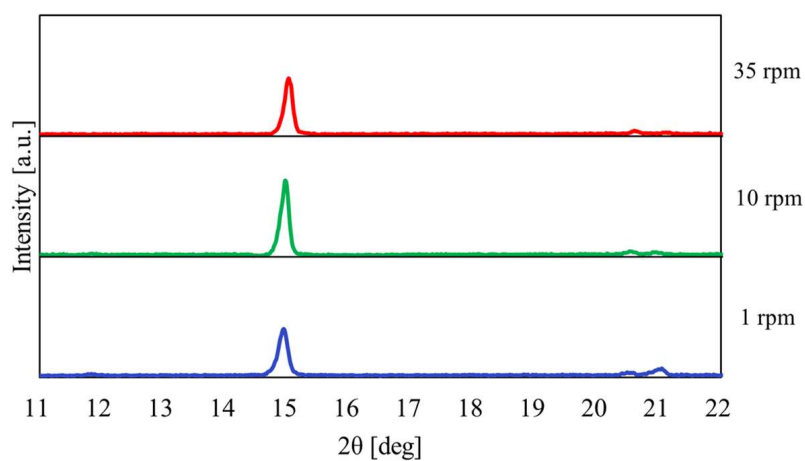
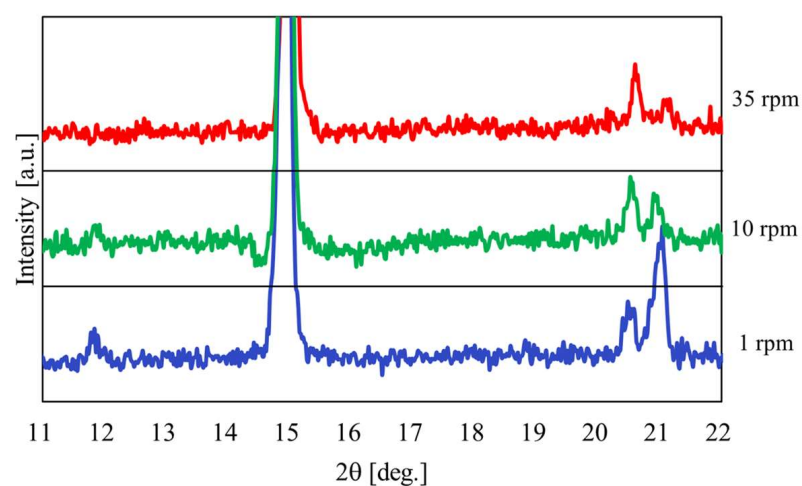


Figure 13. Time histories of temperature and pressure inside the rotary vessel at a heating end temperature of 180 °C when the rotation speed was changed.



(a)



(b)

Figure 14. XRPD measurement results at a heating end temperature of 180 °C when the rotation speed was changed; (a) Normal figure; (b) Enlarged figure.

Table 4 shows the mass fractions of $\text{CaSO}_4 \cdot 2\text{H}_2\text{O}$, $\text{CaSO}_4 \cdot 0.5\text{H}_2\text{O}$, and CaSO_4 under conditions where the heating end temperature was 180°C and the rotation speed was varied. Figure 15 summarizes the mass fractions of $\text{CaSO}_4 \cdot 2\text{H}_2\text{O}$, $\text{CaSO}_4 \cdot 0.5\text{H}_2\text{O}$, and CaSO_4 at each rotation speed. As shown in Figure 15, when the heating end temperature was 180°C and the rotation speed was 1 rpm, the mass fraction of $\text{CaSO}_4 \cdot 2\text{H}_2\text{O}$ was 7.27% and $\text{CaSO}_4 \cdot 0.5\text{H}_2\text{O}$ was 91.48%. This result shows that almost all $\text{CaSO}_4 \cdot 2\text{H}_2\text{O}$ was converted to $\text{CaSO}_4 \cdot 0.5\text{H}_2\text{O}$ under a rotation speed of 1 rpm. Furthermore, the 10 and 35 rpm results show a lower mass fraction of $\text{CaSO}_4 \cdot 2\text{H}_2\text{O}$ than the result of the rotation speed of 1 rpm. Here, under these conditions, the mass fraction of CaSO_4 increased while $\text{CaSO}_4 \cdot 0.5\text{H}_2\text{O}$ decreased. These results show that increasing the rotation speed promotes the thermal dehydration of gypsum and that $\text{CaSO}_4 \cdot 0.5\text{H}_2\text{O}$ begins to be converted to CaSO_4 . The above results confirm that increasing the rotation speed accelerates the heat conduction and heat transfer of the particles in the vessel [13].

Table 4. Results of the mass fraction of $\text{CaSO}_4 \cdot 2\text{H}_2\text{O}$, $\text{CaSO}_4 \cdot 0.5\text{H}_2\text{O}$, and CaSO_4 using Rietveld analysis at a heating end temperature of 180°C when the rotation speed was changed.

N (rpm)	T ($^\circ\text{C}$)	$\text{CaSO}_4 \cdot 2\text{H}_2\text{O}$ ϕ_m (%)	$\text{CaSO}_4 \cdot 0.5\text{H}_2\text{O}$ ϕ_m (%)	CaSO_4 ϕ_m (%)
0	0	93.74	4.14	2.13
1	180	7.27	91.48	1.25
10	180	3.35	76.19	20.45
35	180	1.14	84.00	15.20

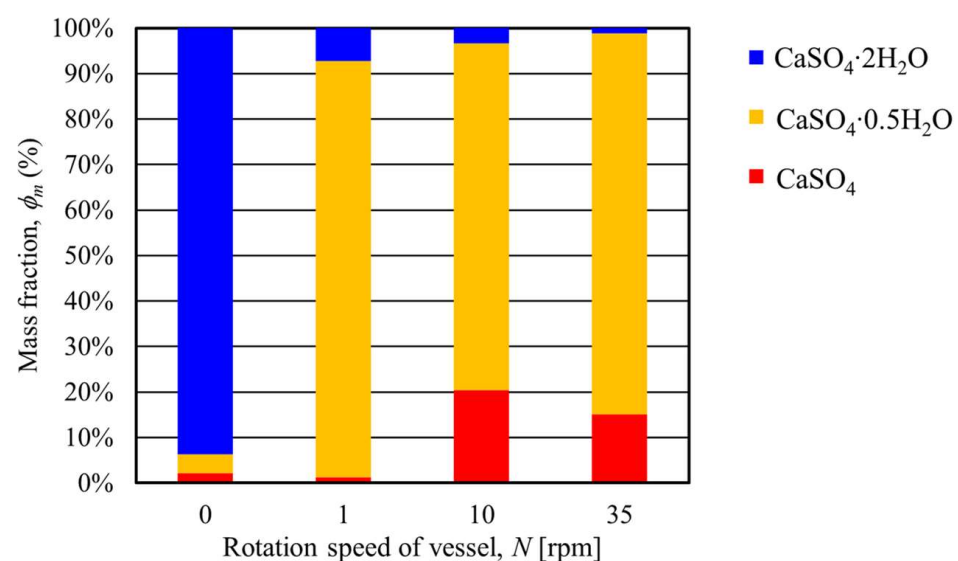


Figure 15. Relationship between the transferring mass fraction of gypsum and the rotation speed of the rotary vessel at a heating temperature of 180°C .

Here, the results of temperature distribution in relation to heating time will be considered. A wave-like periodic temperature change was observed at a rotation speed of 1 rpm. On the other hand, no frequent temperature changes were observed when the rotation speed was 10 rpm or higher. This difference in temperature change at different rotation speeds is related to the gypsum's rotational flow inside the vessel. Therefore, we observed the flow pattern of the gypsum inside the rotating vessel.

Figure 16a shows a snapshot of the inside of the rotating vessel. Figure 16b,c show the schematic diagrams of particle flow based on Figure 16a. As a result, it was confirmed that in a rotating vessel, the gypsum rose along the vessel wall as the vessel rotated. After

that, the particles collapsed and returned to the bottom of the vessel when they reached a certain height. Here, it was found that gypsum particle collapse occurred periodically under low rotational speed conditions, whereas under conditions over 10 rpm, it occurred continuously. It is thought that changes in temperature behavior appeared depending on differences in how the gypsum particles inside the vessel collapsed.

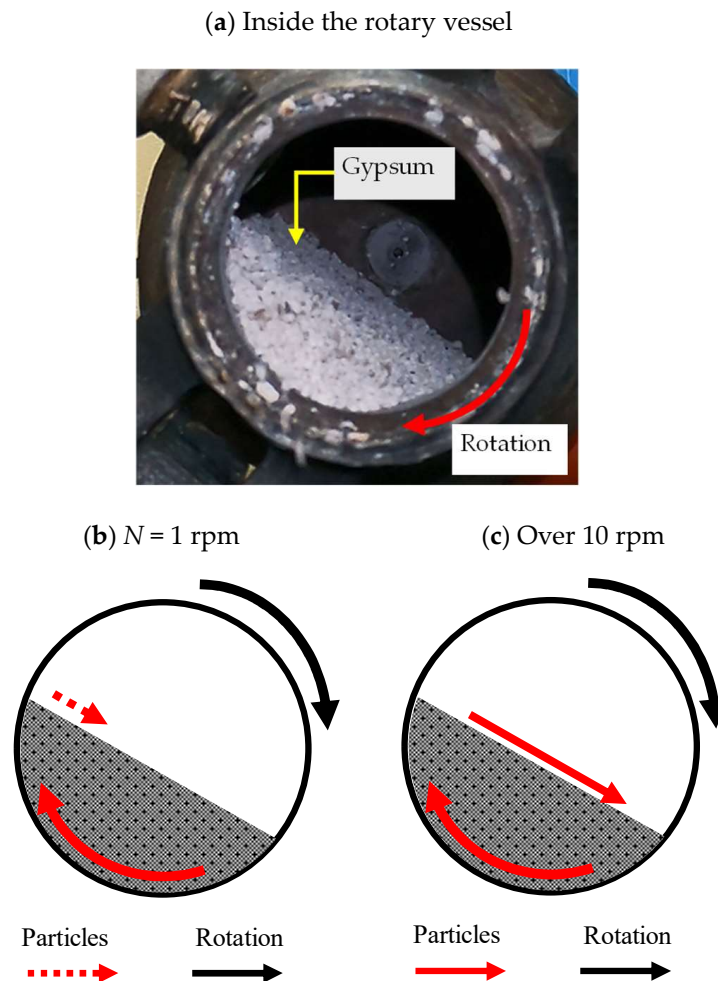


Figure 16. Typical flow pattern of gypsum particles in a rotating vessel.

Figure 17 shows the relationship between the internal pressure of the vessel and the heating end temperature when the rotation speed is varied. Furthermore, Figure 18 shows the relationship between the internal pressure of the vessel and the rotation speed at each heating end temperature. Both figures show that the ultimate pressure inside the vessel increased as the heating end temperature and rotation speed increased. This is because the rotation given to the vessel filled with gypsum promoted the flowability and heat conduction of the gypsum particles, leading to the active desorption of crystallized water. Also, as shown in Figure 18, the internal pressure of the vessel increased as the rotation speed increased until the rotation speed was around 10 rpm. On the other hand, when the rotational speed exceeded 10 rpm, the growth rate of pressure tended to decrease. This trend suggests a limit to the rotation speed for promoting thermal dehydration.

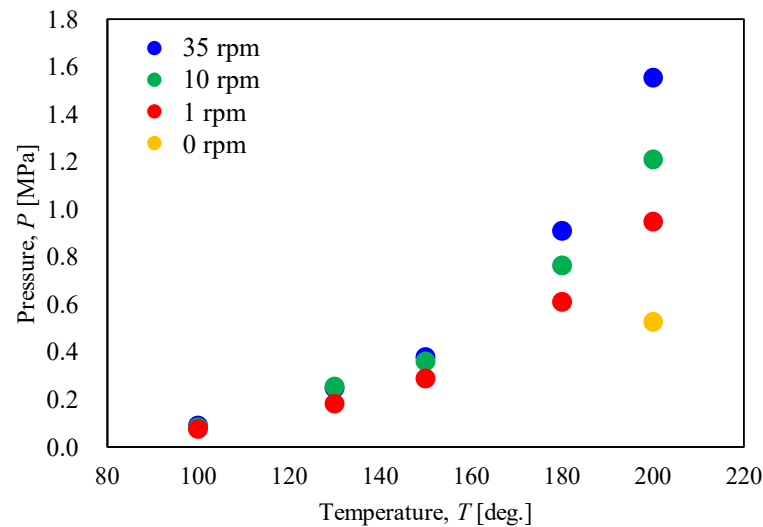


Figure 17. Relationship between the pressure in the rotary vessel and the heating end temperature when the rotation speed was changed.

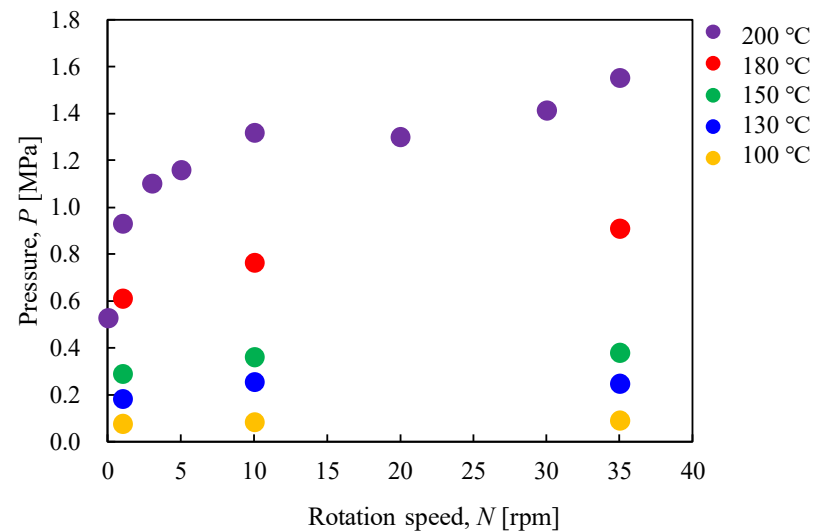


Figure 18. Relationship between the pressure in the rotary vessel and the rotation speed when the heating end temperature was changed.

4. Conclusions

This study investigated the thermal dehydration characteristics of $\text{CaSO}_4 \cdot 2\text{H}_2\text{O}$ using constant-volume rotary heating equipment. The results obtained are shown below.

- (1) It was confirmed that the temperature distribution against the heating time changed due to the difference in the flow pattern of particles in a rotary vessel when the rotation speed was varied.
- (2) Temperature and pressure distribution in regions I to IV depends on the detachment of crystallized water from the gypsum.
- (3) It was found that the desorption of gypsum crystal water was promoted when the rotary vessel's rotation speed was increased. As a noteworthy point, the pressure inside the vessel in region IV increased rapidly. The result indicates that the crystallized water was released from the gypsum.
- (4) We obtained the conversion characteristics of $\text{CaSO}_4 \cdot 2\text{H}_2\text{O}$ to $\text{CaSO}_4 \cdot 0.5\text{H}_2\text{O}$ using a constant-volume rotary vessel. In the present heating equipment, the mass fraction of $\text{CaSO}_4 \cdot 0.5\text{H}_2\text{O}$ increased when the temperature was 180 °C and rotation was applied.

Author Contributions: Conceptualization, K.O. and H.K.; methodology, K.O. and H.K.; formal analysis, investigation, and data curation, K.O., K.A., H.G., K.S. and K.T.; writing—original draft preparation, K.O., K.A., H.G. and K.S.; writing—review and editing, K.T., H.K. and H.S.; visualization, K.O., K.A., H.G., K.S. and K.T.; supervision and project administration, K.O., H.K. and H.S. All authors have read and agreed to the published version of the manuscript.

Funding: This research received no external funding.

Institutional Review Board Statement: Not applicable.

Informed Consent Statement: Not applicable.

Data Availability Statement: Data are contained within the article.

Acknowledgments: A part of this work was supported by the GEAR5.0 project for education and advanced resources at the National Institute of Technology, KOSEN.

Conflicts of Interest: The authors declare no conflicts of interest.

References

1. Kanto Branch of Japanese Geotechnical Society. *Research Report on Applying Soil Improvement Material of Recycling Waste Plasterboard*; Kanrto Branch of Japanese Geotechnical Society: Tokyo, Japan, 2013; pp. 3–19.
2. Horai, H.; Kamei, T.; Ogawa, Y.; Shibi, T. Development of Bassanite Production System and its Geotechnical Engineering Significance -Recycling of Waste Plasterboard. *Jpn. Geotech. J.* **2008**, *3*, 133–142. [[CrossRef](#)]
3. Kamei, T.; Shuku, T. Unconfined Compressive Strength of Cement-Stabilized Soils Containing Bassanite Produced from Waste Plasterboard. *Jpn. Geotech. J.* **2007**, *2*, 237–244. [[CrossRef](#)]
4. Kamei, T.; Kato, T.; Shuku, T. Effective Use for Bassanite as Soil Improvement Materials -Recycling of Waste Plasterboard. *Jpn. Geotech. J.* **2007**, *2*, 245–252. [[CrossRef](#)]
5. Matsuda, H.; Nakashima, K.; Umamoto, M.; Ito, Y. Recycling of Gypsum Waste and used to Ground Improvement Solidification Materials. *Res. Rep. Fac. Eng. Nagasaki Univ.* **2009**, *39*, 28–35.
6. Sano, H.; Yamada, M.; Kotake, N.; Inazumi, S.; Kuwajima, K. Proposal of Estimating Equations on Water Content of Stabilized Soils by Reclaimed Gypsums. *Jpn. Geotech. J.* **2015**, *10*, 603–610.
7. Ahmed, A.; Soliman, A.M.; El Naggar, M.H.; Kamei, T. An assessment of geo-environmental properties for utilization of recycled gypsum in earthwork projects. *Soil Found.* **2015**, *55*, 1139–1147. [[CrossRef](#)]
8. Shigematsu, H.; Nishiki, Y.; Nishizawa, M.; Ikemura, H. Discussion on the lime soil stabilization of acid sulfate soil. *J. Jpn. Soc. Civ. Eng. Ser. C* **2009**, *66*, 425–430. [[CrossRef](#)]
9. Shigematsu, H.; Nishizawa, M.; Yabushita, R.; Yoshimura, K.; Tanaka, H.; Tsuji, K. Mechanical properties od lime stabilized soil with recycled bassanite derived from waste plaster board. *J. Jpn. Soc. Civ. Eng. Ser. C* **2013**, *69*, 272–284.
10. Van Driessche, A.E.S.; Stawski, T.M.; Kellermeier, M. Calcium sulfate precipitation pathways in natural and engineered environments. *Chem. Geol.* **2019**, *530*, 119274. [[CrossRef](#)]
11. Marion, G.M.; Catling, D.C.; Kargel, J.S.; Crowley, J.K. Modeling calcium sulfate chemistries with applications to Mars. *Icarus* **2016**, *278*, 31–37. [[CrossRef](#)]
12. The Society of Inorganic Materials. *Cement, Gypsum and Lime Handbook*; Gihodo Shuppan: Tokyo, Japan, 1996; pp. 138–143.
13. Komossa, H.; Wirtz, S.; Scherer, V.; Herz, F.; Specht, E. Heat transfer in direct heated rotary drums filled with monodisperse spheres: Comparison of experiments with DEM simulations. *Powder Technol.* **2015**, *286*, 722–731. [[CrossRef](#)]

Disclaimer/Publisher's Note: The statements, opinions and data contained in all publications are solely those of the individual author(s) and contributor(s) and not of MDPI and/or the editor(s). MDPI and/or the editor(s) disclaim responsibility for any injury to people or property resulting from any ideas, methods, instructions or products referred to in the content.